Ce- and Ni-codoped Double $PrBaMn_2O_5$ Perovskite as a New Ceramic SOFC Anode

Praveen B. Managutti,[a] Yeting Wen,[b] T.C. Hansen,[c] Vincent Dorcet,[d] Serge Paofai,[d] Pascal Briois,[e] Kevin Huang,[b *] and Mona Bahout [d*]

[a] Chemical Crystallography Laboratory, Khalifa University of Science and Technology, Abu Dhabi, P.O. Box 127788, United Arab Emirates

[b] Department of Mechanical Engineering, University of South Carolina, Columbia, SC, 29208, USA

[c] Institut Laue-Langevin, 71 avenue des Martyrs CS 20156, 38042 Grenoble Cedex 9, France

[d]Univ Rennes, CNRS, ISCR (Institut des Sciences Chimiques de Rennes) - UMR 6226, F-35000 Rennes, France

[e]FEMTO-ST Institute (UMR CNRS 6174), Université Bourgogne Franche-Comté, UTBM, F-25200 Montbéliard Cedex, France

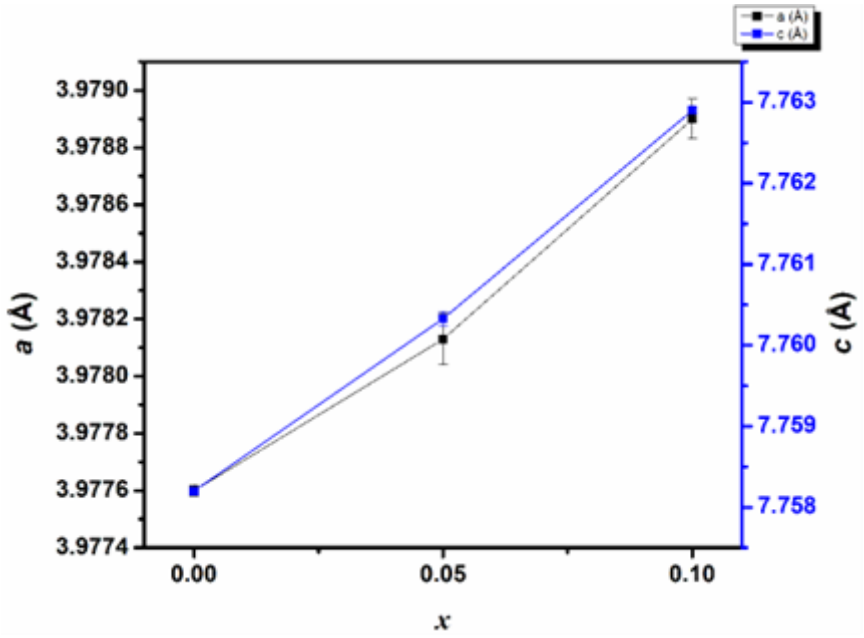

Figure S1. Variation of *a* and *c* lattice parameters for as-prepared $Pr_{1-x}Ce_xBaMnO_5$ as a function of cerium content.

Table S1. Lattice parameters of the as prepared layered perovskites (S.G. *P*4/*mmm*).

	***a* (Å)**	***c* (Å)**	***V* (Å³)**	**O1-*Occupancy***
PBM-H	3.9776 (2)	7.7582 (3)	122.74 (1)	0.1 (1)
PrCe5-H	3.97813 (6)	7.76033 (9)	122.811 (3)	0.03 (6)
PrCe10-H	3.97890 (7)	7.7629 (2)	122.899 (4)	0.04 (8)

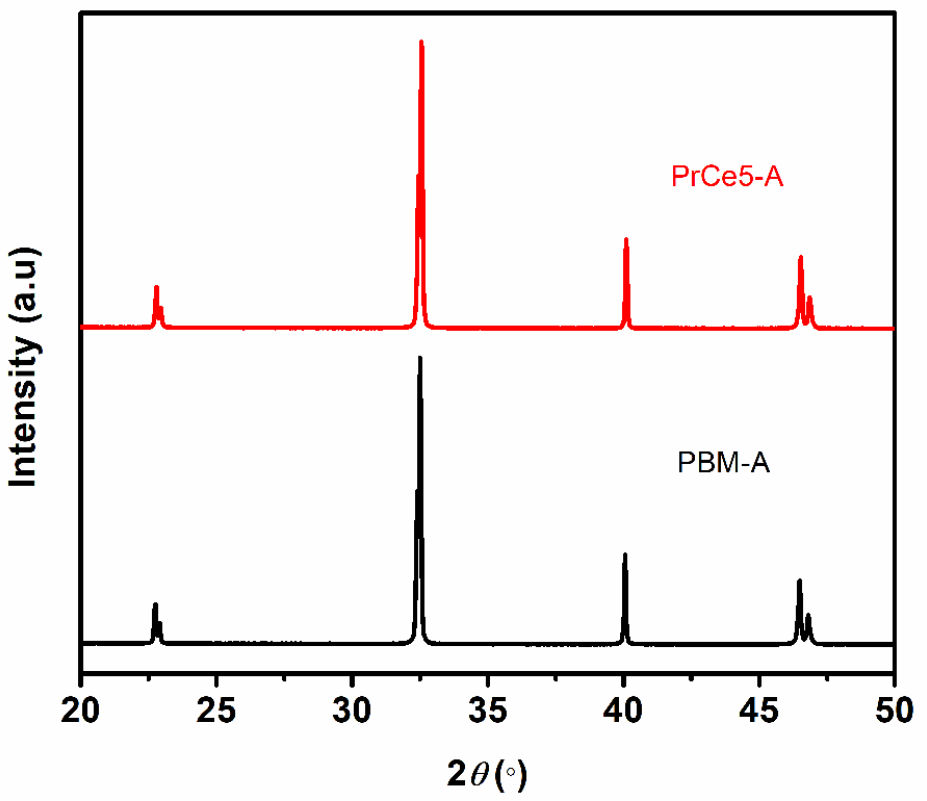

Figure S2. XRD patterns of the layered double perovskites oxidized in air at 800 °C.

Table S2. Structural parameters of the oxidized layered double perovskites (S.G. *P*4/*mmm*).

	***a* (Å)**	***c* (Å)**	***V* (Å³)**
PBM-A	3.90151 (3)	7.75061 (6)	117.978 (3)
PrCe5-A	3.90201(3)	7.75075 (6)	118.010 (3)

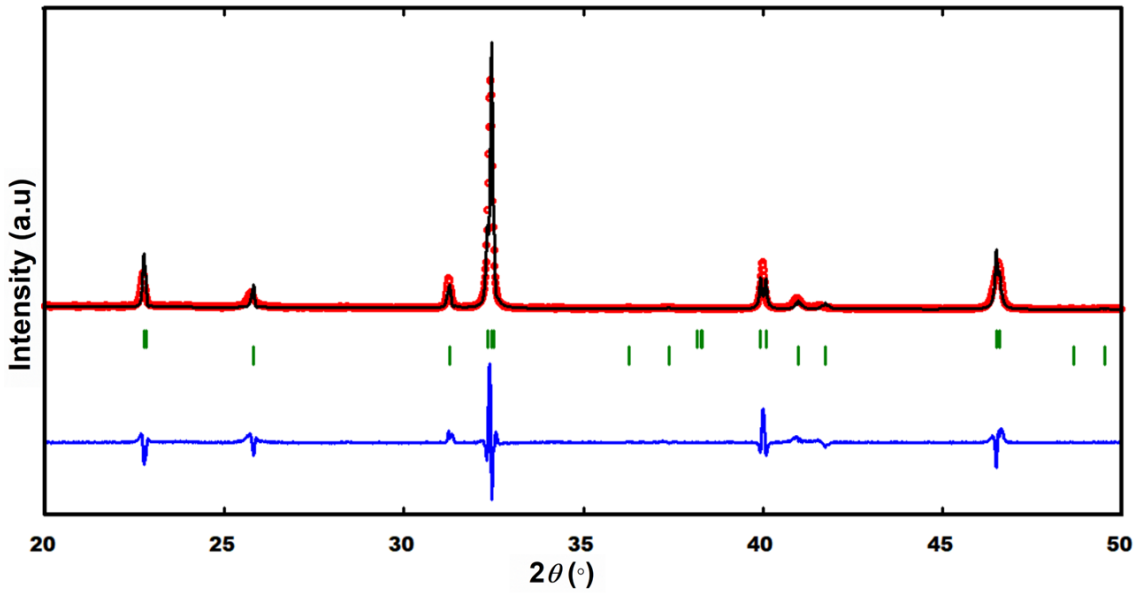

Figure S3. Rietveld refinement for as-prepared PrCe5Ni. Tick marks refer to (upper) (Pr,Ba)$MnO_{3-\delta}$, S.G. *Ibmm*, and (lower) 2H-$BaMnO_{3-\delta}$, S.G. *P*6_3/*mmc*) perovskites.

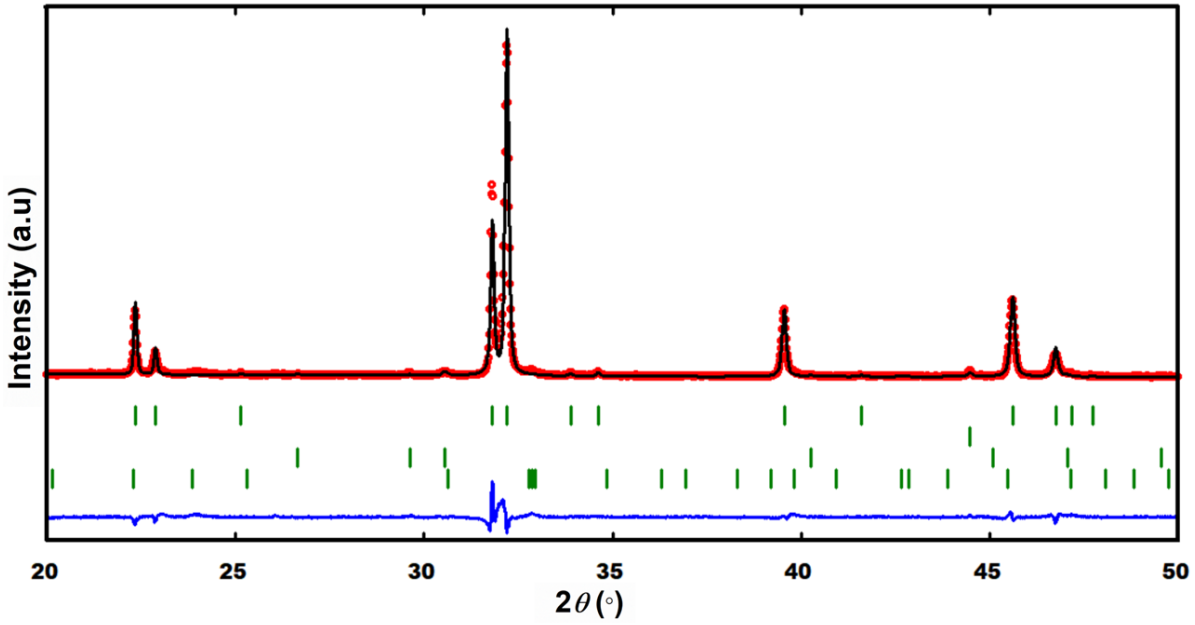

Figure S4. Rietveld refinement for PrCe5Ni after hydrogen reduction at *T* = 875 °C. Tick marks refer to (upper row) PrCe5, (second row) Ni metal, (third row) Pr_2O_3, and (lower row) $PrMnO_3$.

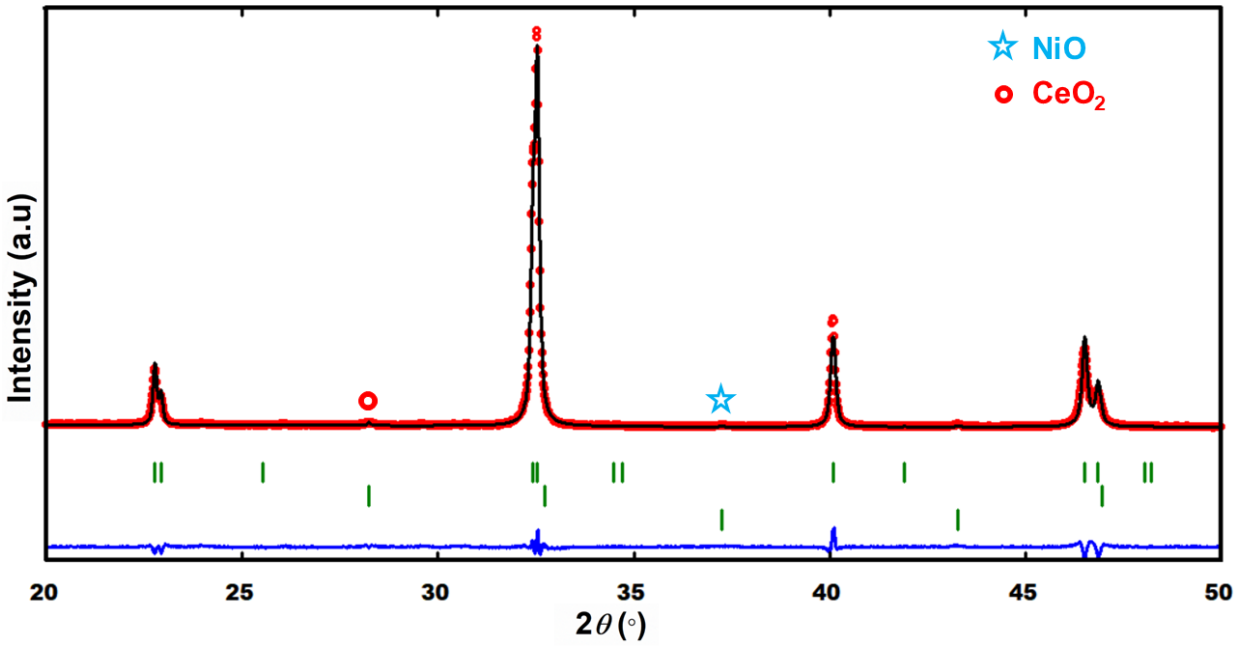

Figure S5. Rietveld refinement for the oxidized PrCe5Ni sample indicating the presence of trace amounts of (red circle) CeO_2 and (blue star) NiO.

.

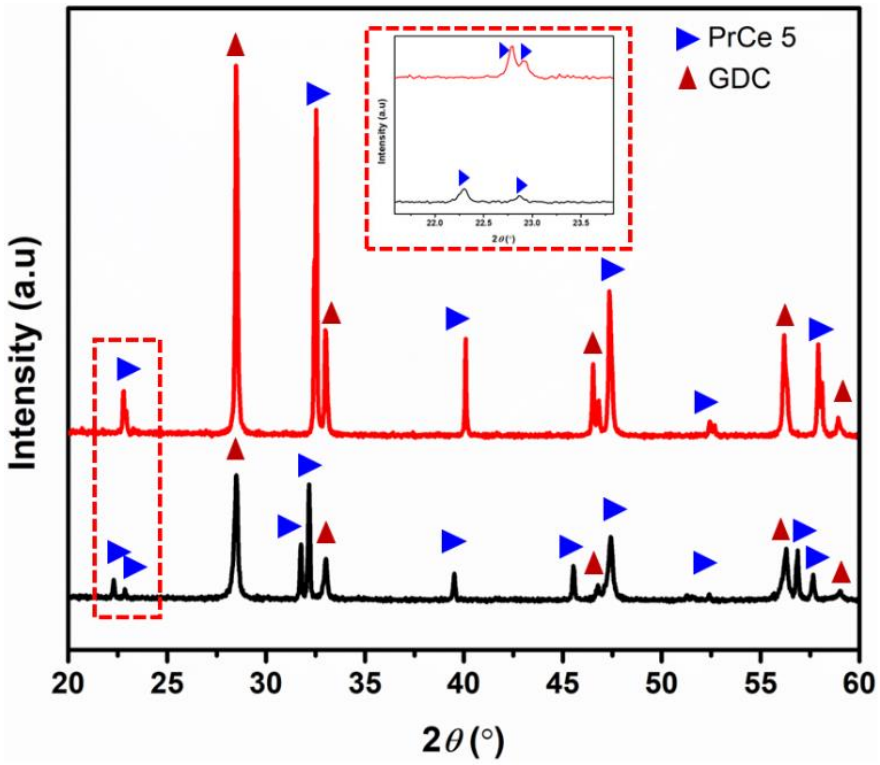

Figure S6. XRD patterns of PrCe5/GDC 50/50w/w (black) before and (red) after heating in air at 1200 °C.

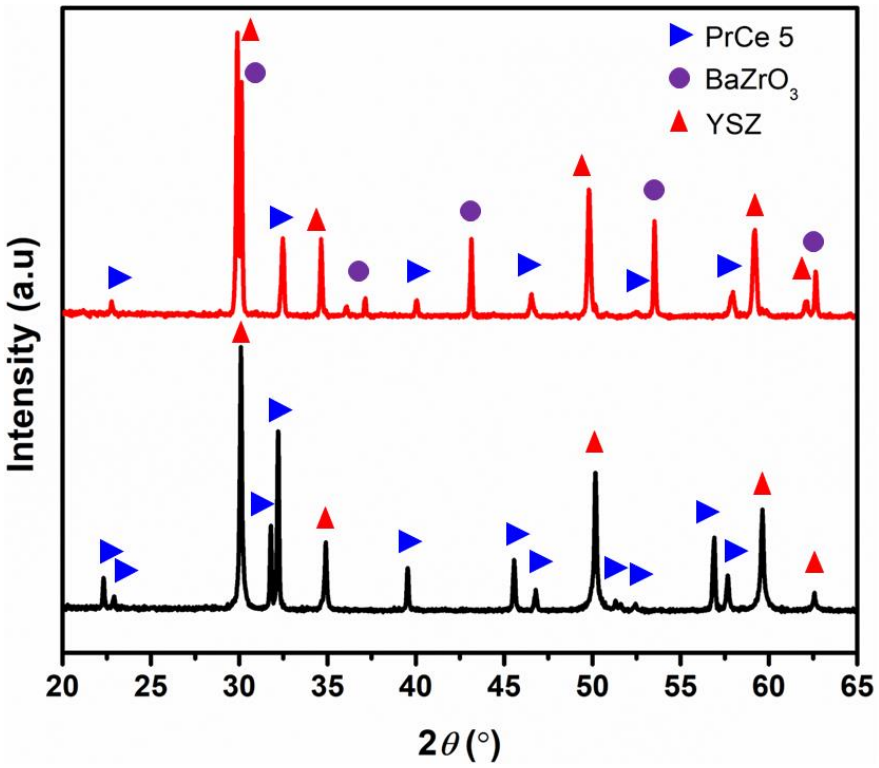

Figure S7. XRD patterns of reactivity tests for PrCe5/YSZ 50/50w/w (black) before and (red) after heating in air at 1200 °C for 3 h.

Table S3. Structural Parameters for PrCe5 determined by Rietveld analysis of NPD at 20 °C in S.G. *P*4/*mmm*, *a* = 3.9653 (1) Å, *c* = 7.7473 (3) Å.

atom	***site***	***x***	***y***	***z***	B_{iso} (Å^2)	***occ.***
Pr/Ce	*1a*	0	0	0	1.0(2)	0.97/0.03
Ba	*1b*	0	0	0.5	2.2(2)	1
Mn	*2h*	0.5	0.5	0.2418(7)	0.9(1)	1
O1	*1c*	0.5	0.5	0	1.4(2) *	0.024(1)
O2	*1d*	0.5	0.5	0.5	1.4(2) *	1
O3	*4i*	0.5	0	0.1961(3)	1.1(0)	0.99(2)

* Constrained to be the same.

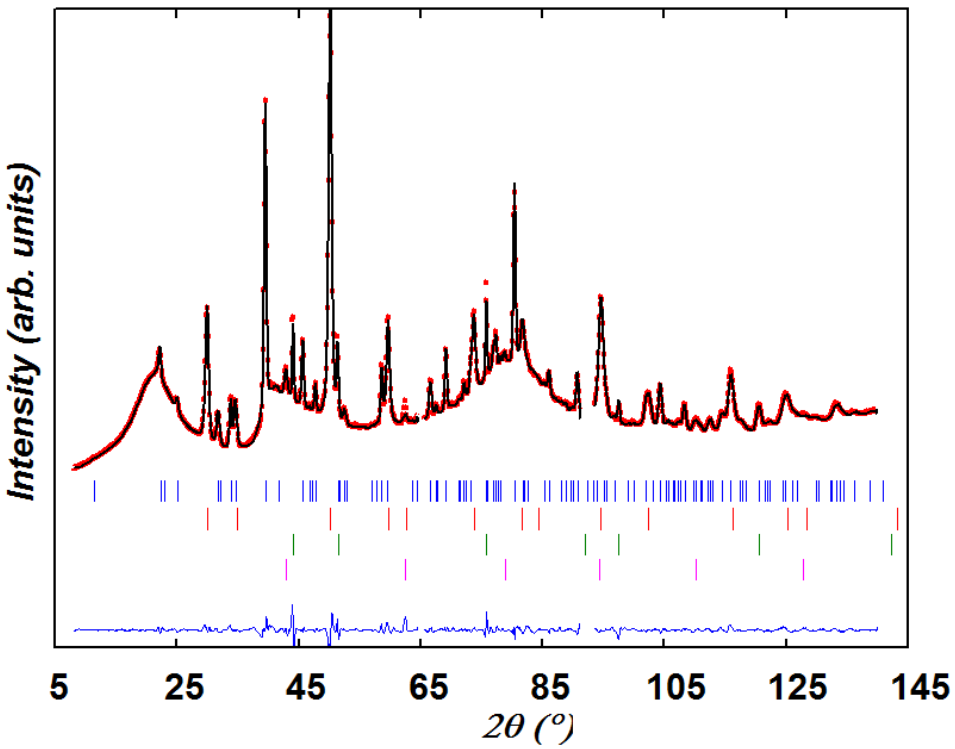

Figure S8. Neutron Powder Diffraction (NPD) pattern of PrCe5/8YSZ composite collected at 20 °C, using a wavelength of 1.54 Å. Tick marks indicate phases from PrCe5 (first row) and YSZ (second row). The presence of the Chromel-Alumel thermocouple (S.G. *Fm*-3*m*, third row) and the vanadium heating element (S.G. *Im*-3*m*, fourth row) is also noted.

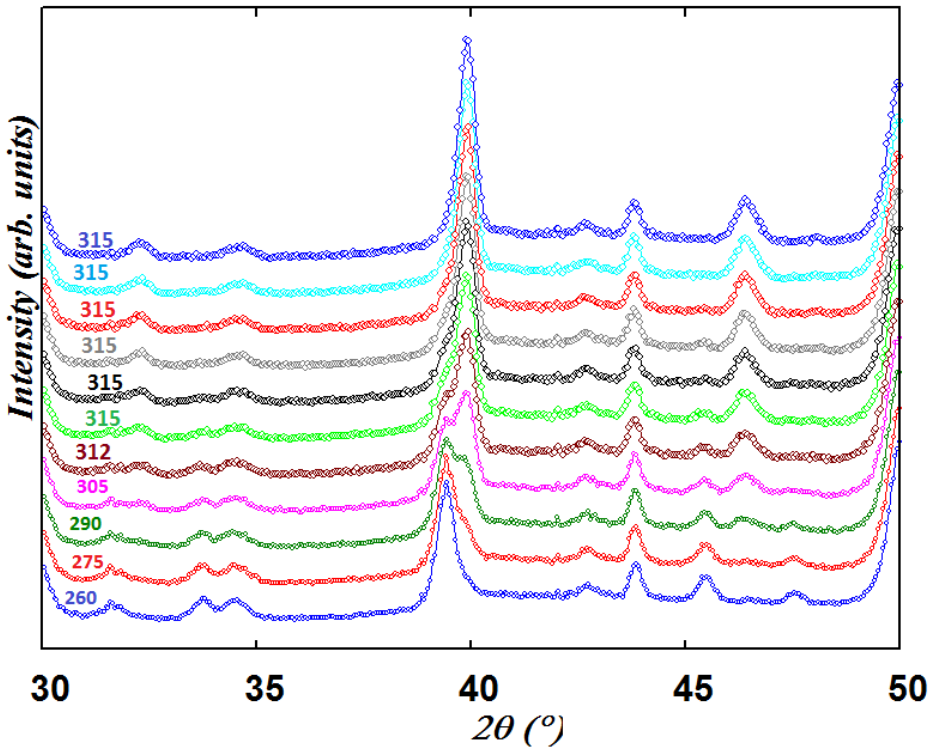

Figure S9. Neutron Powder Diffraction (NPD patterns of PrCe5/8YSZ composite collected in air within the oxidation temperature range using a wavelength of 1.54 Å. Temperature increases upwards.

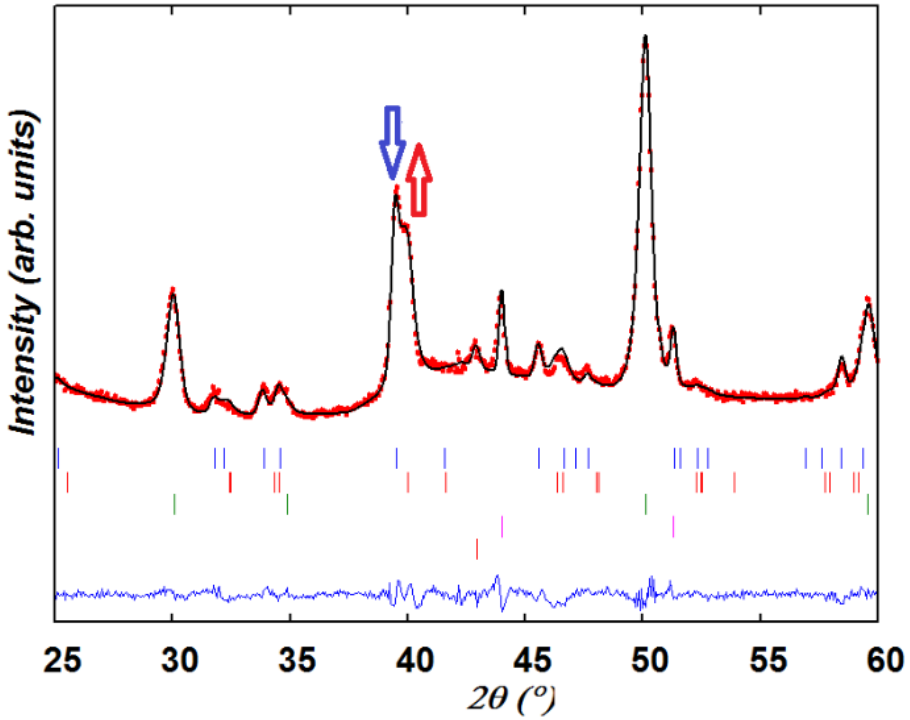

Figure S10. Rietveld analysis of the neutron data (λ = 1.54 Å) collected at 290 °C upon heating in air the progression of reduced (blue, first row) and oxidized (red, second row) PrCe5 phases. Contributions from the YSZ electrolyte (3rd row), the thermocouple (4th row) and vanadium heating element (5th row) are shown.

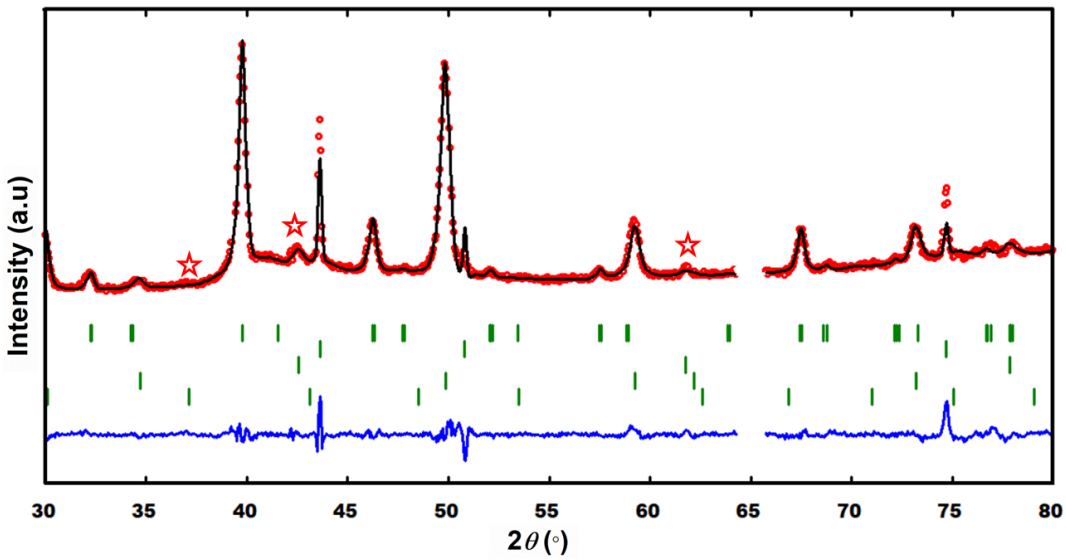

Figure S11. NPD patterns for PrCe5/8YSZ at T = 950 °C highlighting main peaks from $BaZrO_3$ (4th row). The tick marks for PrCe5 (1st row), 8YSZ (2nd row), and the thermocouple (3rd row) are delineated.

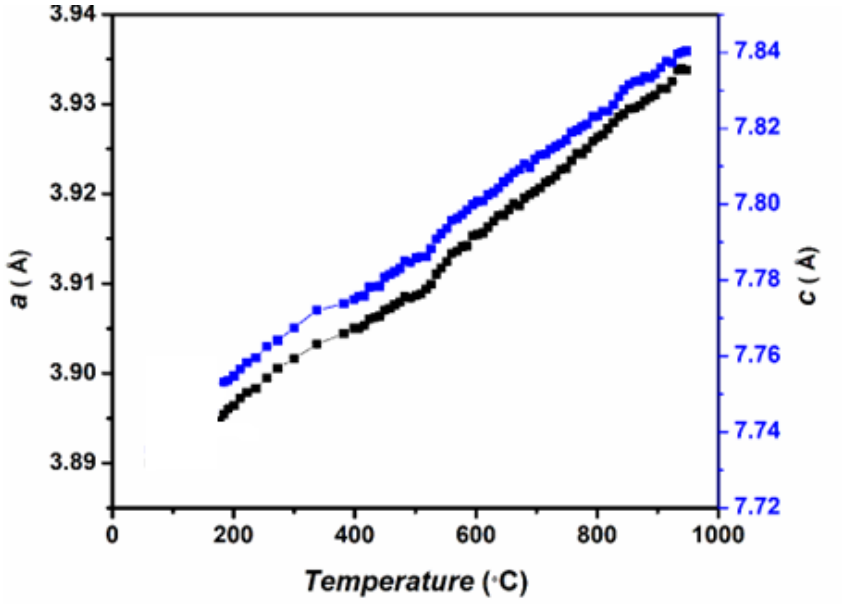

Figure S12. Lattice parameters *a* (in black) and *c* (in blue) for PrCe5, as determined from Neutron Powder Diffraction measurements during cooling in air.

a *b*

Figure S13. Comparison of 8 µm-GDC buffer layer on YSZ substrate: (a) intact and uniform layer pre-testing, (b) delamination and peeling post-testing due to thermal expansion mismatch.

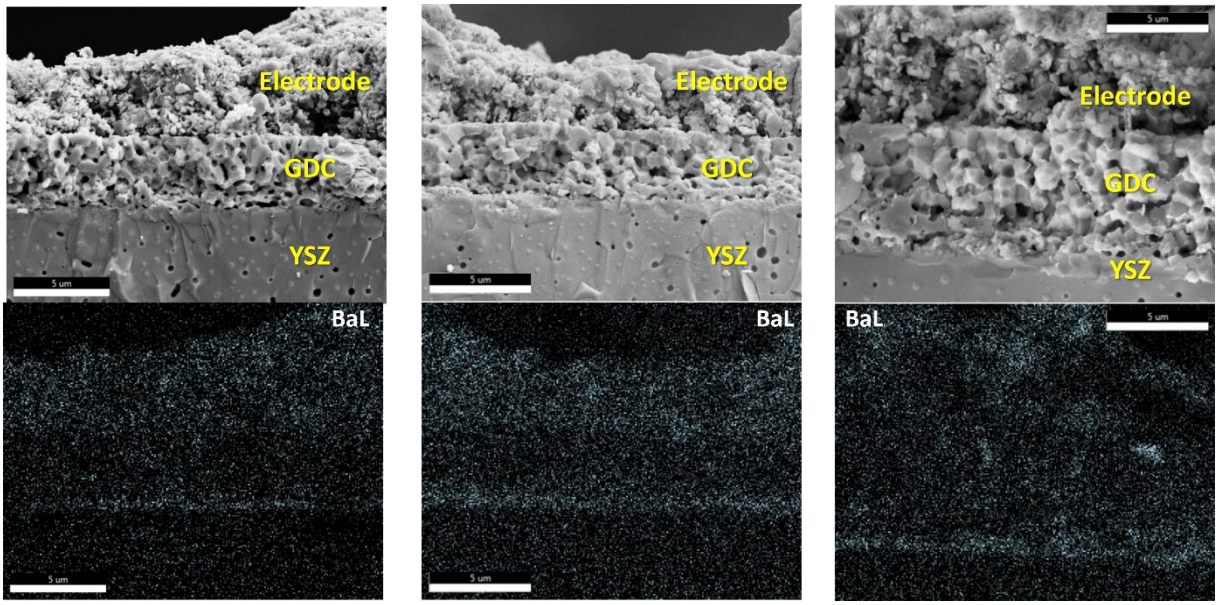

Figure S14. PBM electrode cross-section SEM images on 3.5-GDC coupled with EDS barium mapping taken from various baseline locations after 200-h hydrogen testing. The extent of Ba migration across the GDC buffer layer underscores potential impact on the electrode's stability and performance.

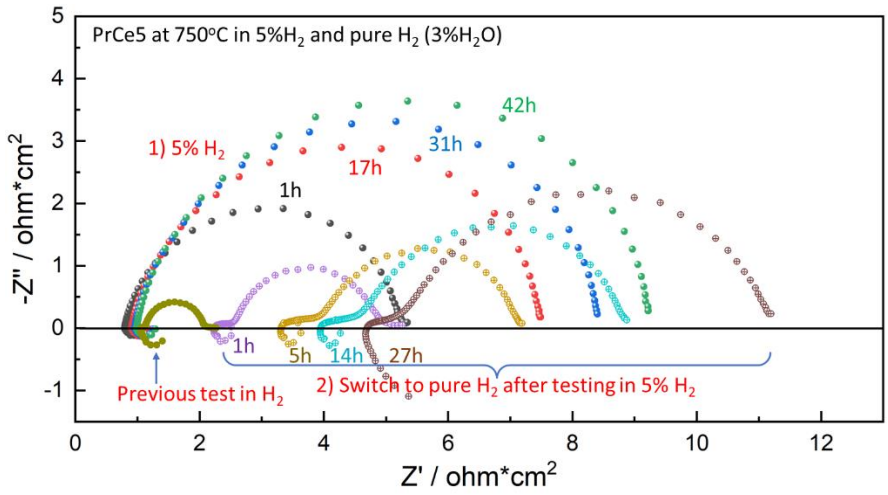

Figure S15. Nyquist plot for PrCe5 electrode screen-printed on a 1 µm-GDC suggest that switching from pure H_2 to 5% H_2 at 750 °C results in increased polarization resistance and irreversible degradation, as evidenced by persistent ASR elevation and spectral shifts.

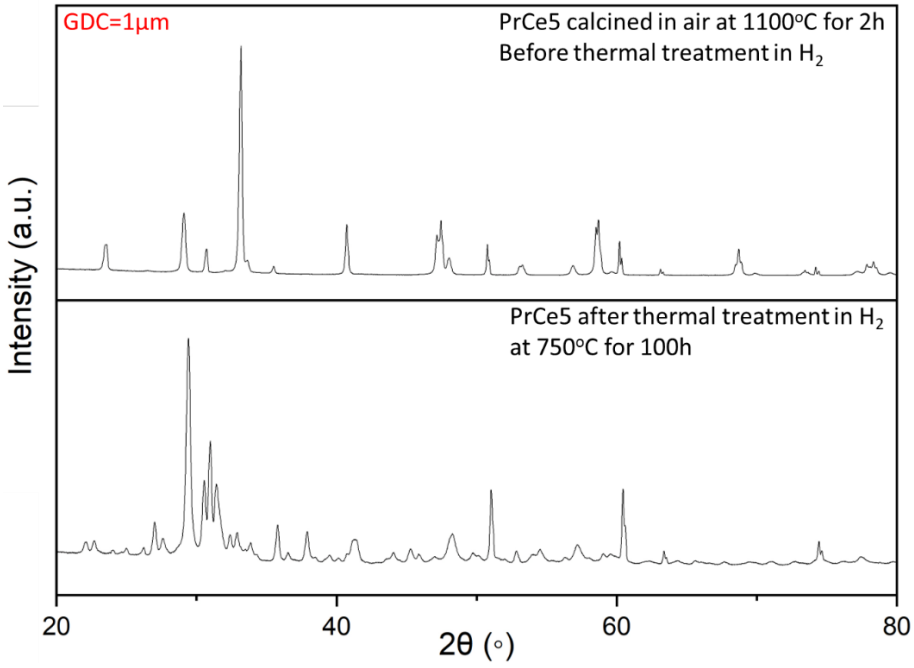

Figure S16. XRD before and after treatment in H_2 for PrCe5 calcined on 1 µm-GDC at 1100 °C. The degradation suggests the migration of the Ba^{2+} ions to the YSZ electrolyte facilitated by the slim GDC buffer layer.

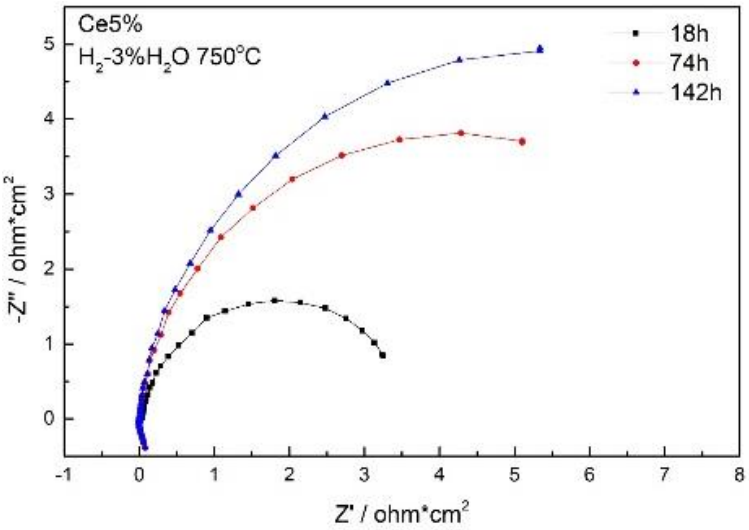

Figure S17. Time evolution of the electrochemical performance of PrCe5/8 µm-GDC. The semicircular shape of the plots indicates a single relaxation process or a single time constant but the shift to the right as the exposure time increases suggests an increase in the material's resistance.

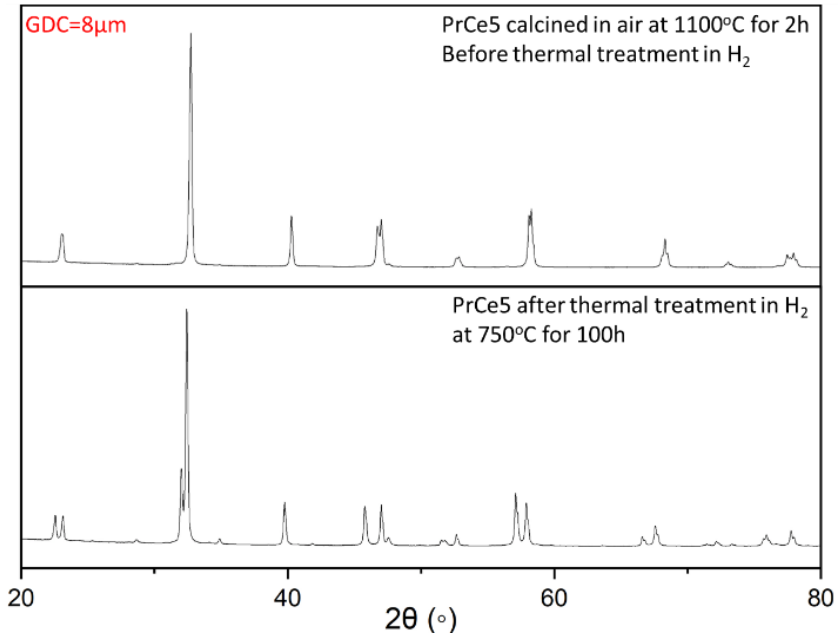

Figure S18. XRD patterns for PrCe5 electrode sintered on 8 µm-GDC before and after treatment in H_2. The comparable array of peaks suggests that the crystalline structure is retained and absence of new phases.

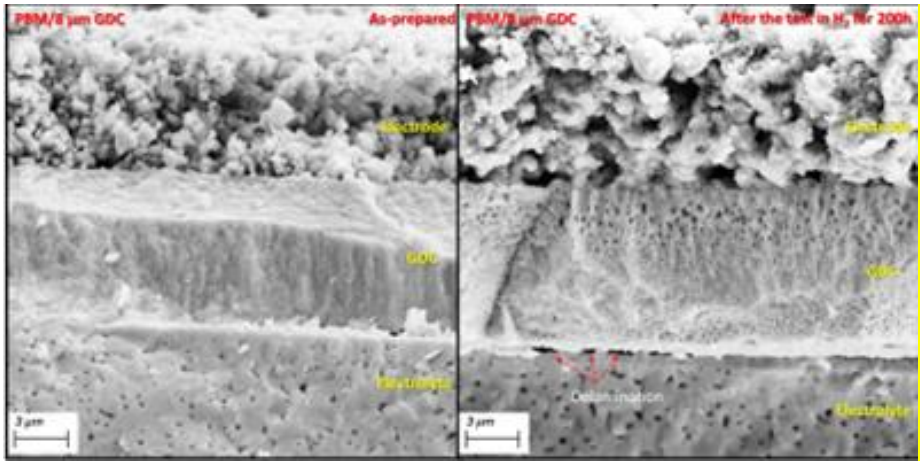

a ***b***

Figure S19. Cross-section SEM for PBM sintered on 8 μm-GDC before and after 200h H_2 testing.